

# Millimeter Wave Radar for High Resolution 3D Near Field Imaging for Robotics and Security Scans

Sandra Nowok, Simon Kueppers, Harun Cetinkaya, Martin Schroeder,  
Reinhold Herschel

Department of Integrated Circuits and Sensor Systems  
Fraunhofer Institute for High Frequency Physics and Radar Techniques FHR  
Fraunhoferstraße 20, 53343 Wachtberg, Germany  
email: sandra.nowok@fhr.fraunhofer.de

**Abstract:** This paper presents different millimeter wave systems for robotic mapping and localization as well as for security scan applications. The 2D system in the first part of this paper is mechanically rotating the radar module to allow a continuous revolving FMCW radar beam in azimuth plane. This extracted data is compared with the data of a LiDAR system. In the second part 3D imaging systems are presented based on synthetic aperture radar and MIMO arrays.

## 1. Introduction

The main advantage of radar systems is the ability to operate in adverse weather and environmental conditions compared to optical sensors such as lasers. Therefore, radar systems become more interesting concerning localization and mapping in robotics application [1]. One example is the Horizon2020 project Smokebot, where fire and smoke create a dangerous situation for human life. A mobile platform equipped with a sensor suite that is able to handle harsh conditions, is sent in to record the map necessary for operational planning and orientation [2]. For near object inspection radar systems can also be used to scan suspicious-looking objects to analyze for their content [3].

To build a compact radar system, the silicon-germanium (SiGe) technology is used. Thus, a realization of complex analogue and digital circuits up to 240 GHz is possible and therefore a frequency modulated continuous wave radar-chip with integrated analogue signal processing has been developed at the Ruhr University in Bochum in conjunction with the Fraunhofer FHR [4] with dimension of 2x2 mm. This design is already highly interesting for high number of applications in robotics and security scans.

This article is organized as follows. In Section 2. the functionality of a mechanically pivoting radar (MPR) is described. Additionally, the experimental evaluation of the 2D MPR is shown using an indoor measurement site with 2 different objects. Afterwards, the result of data fusion with LiDAR and Radar data is presented. Section 3.1. and 3.3. describe the 3D systems based on synthetic aperture radar and MIMO arrays.

## 2. 2D system

As a simple approach for screening the environment a mechanically pivoting radar (MPR) module was developed. It monitors the distance to reflecting targets within a focused beam. By constantly rotating over time reflection profiles are measured for all azimuth angles around the radar. This can be used to support optical LIDAR systems in case of low visibility caused by fog or smoke. The mechanically pivoted radar is based on a compact USB controlled 80 GHz FMCW radar module (see Figure 1). The module does not exceed 5 cm in all dimensions. Only connected by a standard USB connector it can be easily integrated in a mechanical setup forming a complete radar module. The extremely small form factor is possible by using a integrated radar chip in SiGe technology. This MMIC has a maximum bandwidth of 25 GHz in a frequency range of 78 GHz to 92 GHz and according to this it provides a range resolution of about 6 mm. In order to allow a continuous revolving FMCW radar beam in the azimuth plane, a slip ring is

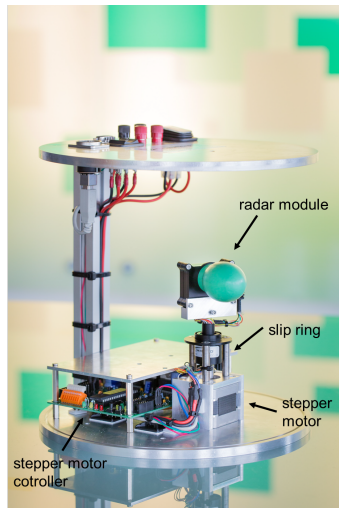


Figure 1: Mechanically Pivoting Radar

used up to the USB power and data lines. The rotation of the radar module is realized using a stepper motor, which is controlled via a commercial available stepper motor controller. The overall mechanical dimensions are 250 mm in diameter and 275 mm in height.

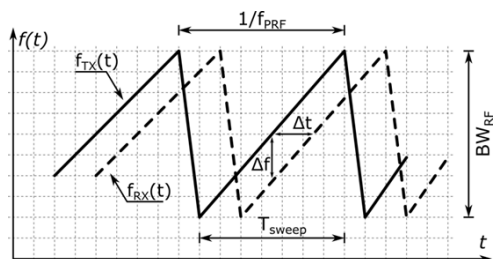


Figure 2: FMCW Radar System working principle

The operation principle of the MPR for a single stationary target reflection is shown in Figure 2. The figure illustrates a transmitted signal (solid line) with a momentary transmit frequency

$f_{TX}(t)$  which changes linearly over time. The linear frequency sweep is described with the frequency bandwidth of  $BW_{RF}$  over  $T_{sweep}$ . This signal is radiated using an antenna and the reflected signal is received with a time delay of  $\Delta t$  from a single target is indicated by the dashed line. On this basis the relationship between the target distance  $R$  to the time delay can be described by Equation 1:

$$R = \frac{c}{2} \cdot \Delta t \quad (1)$$

Due to the linear modulation, the received signal has a specific frequency offset  $\Delta f$  at each point in time during a frequency sweep. This frequency offset has a direct relationship to the time delay  $\Delta t$ , which is a proportional factor of  $BW_{RF}/T_{sweep}$ . Therefore the distance  $R$  can be expressed with the frequency difference  $\Delta f$  as:

$$R = \frac{c \cdot T_{sweep}}{2 \cdot BW_{RF}} \cdot \Delta f \quad (2)$$

To extract this information, the received signal has to be downconverted by a frequency mixer. The intermediate frequency (IF) signal is a linear superposition of all targets visible by the radar. This signal is then digitized and using the Fast-Fourier-Transform algorithm and finally a peak detection to receive the range information for all targets.

Measurement range	up to 15 m
Frequency range	78 GHz to 92 GHz
Sweep time	1 ms
Angular resolution	1.8°
Beam width	4.9°
Scan rate	2.5 Hz

Table 1: Main parameters of the MPR

In Table 1 the main MPR parameters are shown. Due to the rotary resolution of 1.8°, 200 measurements can be done during one rotation of the radar system. The maximum scan rate of 2.5 Hz leads to 500 single radar measurements per seconds, while the radar is continuously scanning in azimuth plane. The MPR is able to measure targets between a range of 0.3 m to about 15 m.

## 2.1. Measurements

To evaluate the imaging capabilities of the MPR, an indoor measurement was performed. Two main object (a trihedral reflector and a person model) were used (right in Figure 3). On the left side of Figure 3 their position within the room is shown. The MPR was placed 3 m from the front door entrance and in directly in front of a side wall. The stepper motor as well as the radar modul was controlled using a remote control.

The trihedral reflector was placed with 2.7 m distance at an azimuth angle of -10° in front of the MPR. This provided a strong reflection at a defined point in space which can be seen as a

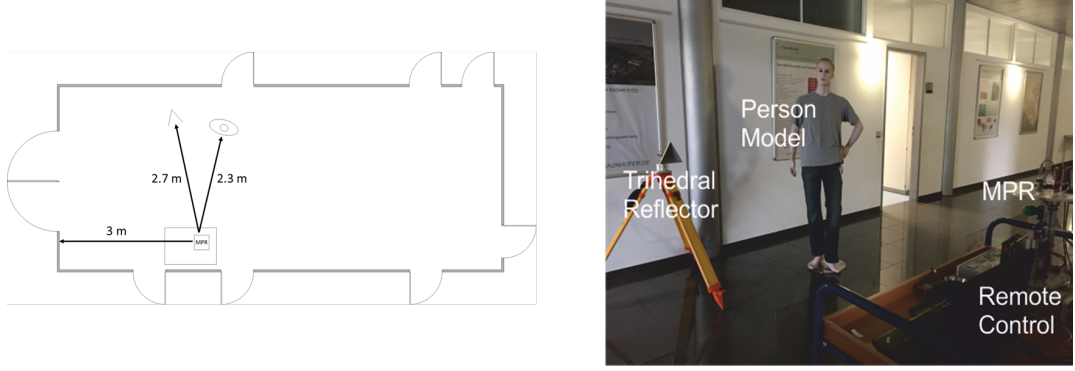


Figure 3: Measurement scene: Outline of measurement site (left); Measurement Setup (right)

dirac impulse in the spatial domain. A person model made out of polymer was taken in order to show the performance of the MPR for more complex objects.

On the left side of Figure 4 the normalized reflected power caused by the trihedral reflector is shown as a function of range while the azimuth angle was fixed to  $-10^\circ$  and the bandwidth was set to 5 GHz. At the leftmost side of the plot, the reflections of the dielectric lens can be observed. This strong reflections also lead on to multiple reflections within the antenna structure so that a range of about 30 cm is covered by the impulse response of the MPR. The chirp bandwidth of 5 GHz causes a 3 dB width single reflection of 3 cm. Using a hanning window in time domain, sidelobes are effectively suppressed.

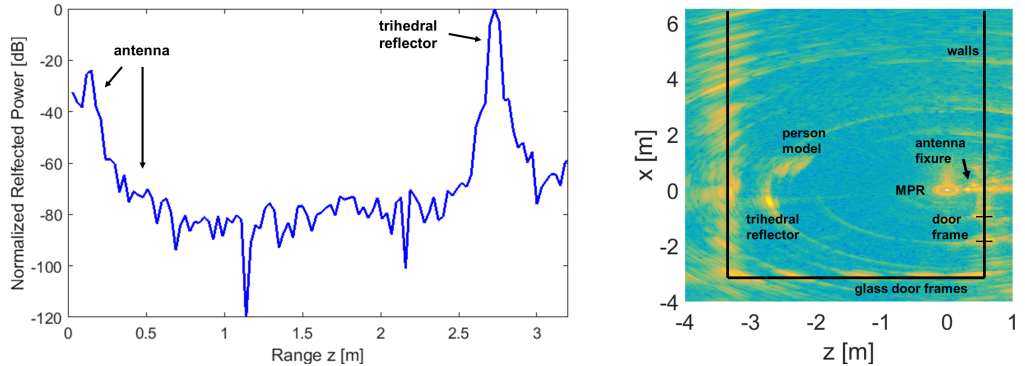


Figure 4: Measurement: Range Profile (left),  $360^\circ$  image in indoor environment using a bandwidth of 5 GHz (right)

The MPR provides two-dimensional information  $360^\circ$  around the robotic platform. On the right in Figure 4 the geometrical structure in the image is similar to the measurement scene in Figure 3. The MPR itself can be clearly identified by the circular structure in the center of the image caused by the reflection at the dielectric antenna surface. On the right, close to the MPR, a strong reflection can be observed. This is the metal strip, which is the mechanical fixture of the MPR (see Figure 1). It is also used for the azimuth angle reference and is measured every  $360^\circ$  turn. The surrounding walls can clearly be seen. In the lower right, the door frames lead to visible reflections.

## 2.2. Test results

During a rescue scenario, in which the visibility can be restricted by dangerous gases, smoke or dust, the risk for an emergency teams has to be reduced. In [5] the Institute of Systems Engineering developed a data fusion method to combine LiDAR data with radar data. They generated artificial smoke within a yard to simulate low visibility conditions. In Figure 5 on the left the integrated system with LiDAR and radar is shown. In the center of this Figure, only the LiDAR data is shown. It reveals the presence of fog, which is marked with red circles. As can be seen in Figure 5 (right), the LiDAR points, which are effected by the fog, are replaced by radar points in the fused image. This clearly underlines how crucial the radar module is under restricted visibility.

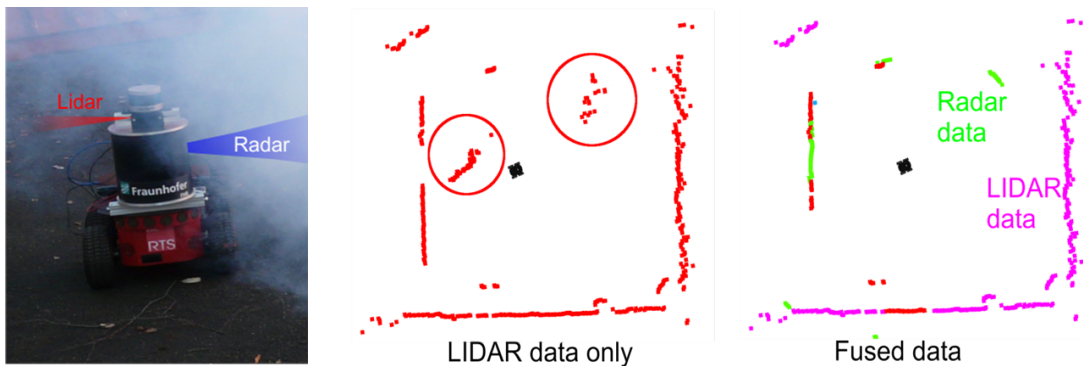


Figure 5: Data Fusion with Lidar and Radar; Integrated System (left), LIDAR data only (center), fused data (right)

## 3. 3D-Systems

To generate a 3D image, a mechanically pivoting in elevation and azimuth would have to be done.. This can also be realized electronically by using an antenna array. In the following two approaches are proposed.

### 3.1. 3D SAR scan Module

The SAR scan module (see Figure 6) uses one channel to create an antenna array by moving it in x and y direction. Therefore, a high resolution image can be generated. The resolution is given by wavelength aperture size and distance to the object. To enable integration to robotic platforms a small aperture scanner was developed.

This system uses the same radar module as mentioned in Section 2. The only difference between them consist on the size of the antenna, which was specially designed for this scan-unit. The 3D printed antenna has a beam width of 22°. The directive character suppresses the clutter from other look angles, but does not restrict the obtained resolution if 50 cm distance between scanner and object is maintained. The scan-unit itself consists out of two guiding rails with two

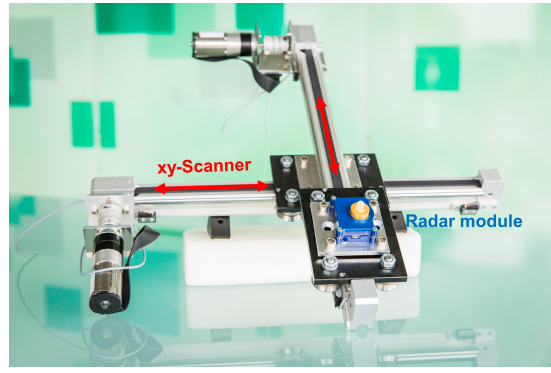


Figure 6: SAR-Scan Module

guiding carriage on which the radar module is mounted. The scanner with the radar module is moving in the y direction with a speed of  $0.0015 \text{ m s}^{-1}$  and in x direction with a speed of  $0.15 \text{ m s}^{-1}$  mounted on a metal stand. During the continuous movement of the guiding carriage, the measurements are performed. The scanning area has a size of 0.25 m by 0.25 m. Figure 7 shows the trajectory (red), how the measurement takes place.

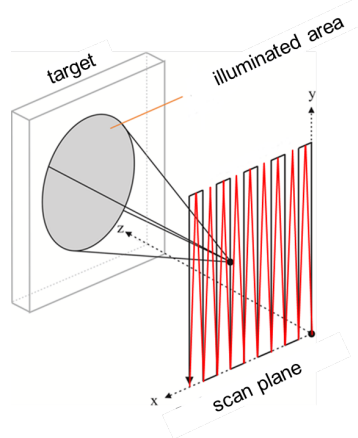


Figure 7: Trajectory

After receiving the IF signal of all measurements, an algorithm such as matched filter, backprojection or range migration algorithm can be used to create the image. Depending on the algorithm the processing time can be reduced drastically, but also the resolution will be reduced.

Measurement range	up to 15 m
Frequency range	78 GHz to 92 GHz
X and Y resolution	2.5 mm
Beam width	$22^\circ$
Scan speed X	up to $0.15 \text{ m s}^{-1}$
Scan speed Y	$0.0015 \text{ m s}^{-1}$

Table 2: Main parameters of the 3D SAR scan module

In Table 2 the main SAR scan module parameters are shown. With a speed of  $6 \text{ cm s}^{-1}$  in x direction and a speed of  $6 \text{ mm s}^{-1}$  in y direction one measurement takes about 7 minutes. There are 10100 measurements positions by a resolution of  $0.0025 \text{ m}$  in x and y direction. The SAR scan module is able to measure targets between a range of  $0.3 \text{ m}$  up to  $15 \text{ m}$ . The overall mechanical dimensions are 472 mm in width and height and 120 mm in depth.

### 3.2. Measurement

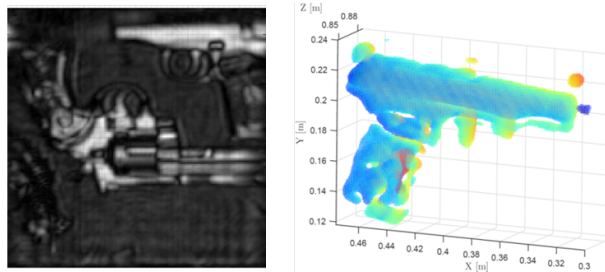


Figure 8: Measurement of weapons (left) and 3D reconstruction (right)

On Figure 8 you see on the left a Measurement of 3 weapons. In the left corner there is a grenade, in the middle a revolver and in the above right a gun. On the right side of Figure 12 there is an 3D reconstructed image of the gun.

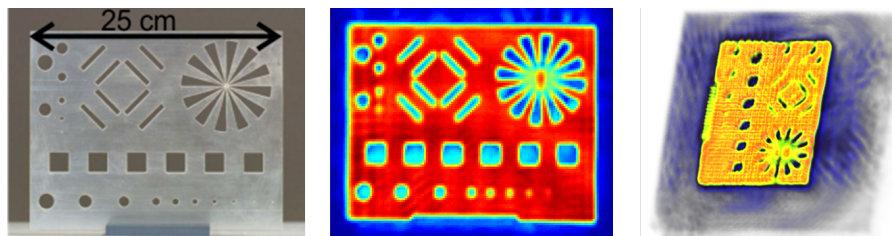


Figure 9: Reference object with several geometrical shapes (left), measurement result (center), 3D visualization (right)

To demonstrate the resolution of the scanner a reference object was made. As shown in Figure 9 this is a 3D printed plastic plate containing several geometrical shapes such as a Siemens star in the upper right corner. In the center of this image, the result of a measurement is shown. Only the last little circle in the last row is not visible in the radar image, because it is too small and fits not into the sampling due to the resolution of the measurement. On the right of Figure 9 a 3D visualization of the measurement is shown, using the reflection coefficient to scale the transparency of each voxel within the reconstructed volume. This clearly underlines the capabilities of millimeter wave scan for 3D imaging.

### 3.3. 3D MIMO Camera

A major drawback of SAR systems is the very long measurement time caused by the sequential measurement of all antenna elements of a complete monostatic array. To enhance the measure-

ment speed a certain level of parallelisation is needed. This can be efficiently realized by multi antenna arrays. Multiple-Input-Multiple-Output (MIMO) arrays are a bistatic concept where each receiver detects signals from various transmitters. To enhance the number of measurements per receiver it is crucial that the signals of each transmitter can be distinguished after being detected at the receiver. To ensure this, orthogonal signals are used for each transmitter. This can be done by frequency, time or code multiplex. For the presented design time-multiplex is used so that each transmitter is only active at a certain time-slot. The image is formed after all transmitters have been active.

All transmitter and receiver combinations form a virtual array, representing the antenna elements of an equivalent monostatic array. Mathematically, the virtual array is the convolution of transmitter and receiver array. A physically sparse MIMO array can be used to form a dense virtual array. This is of great interest to design radar front-ends at millimeter wave frequencies since it allows to increase the spacing of antenna elements to provide space for transmission lines, antenna structures and additional front-end circuitry. The second result of the convolution is the fact that the resulting virtual array appears larger than the physically realized MIMO array. As discussed before the aperture size determines the image resolution at a given distance. Using MIMO technology can therefore also help to minimize the module size for elegant compact and light-weight hardware.

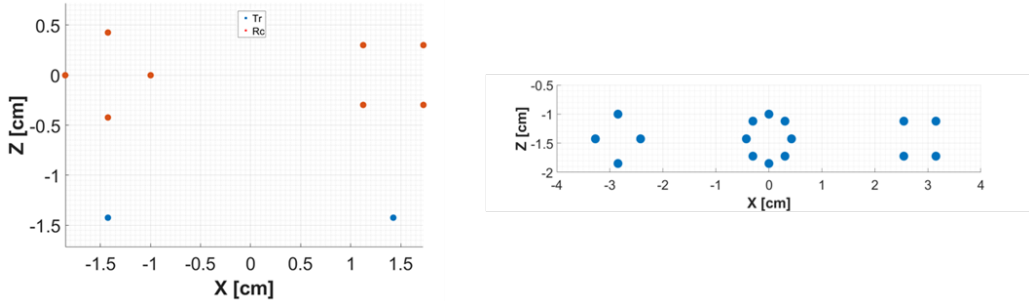


Figure 10: MIMO-Camera: MIMO array design (left), Virtual array created by MIMO design (right)

On the left in Figure 10 the topology for the MIMO camera is shown. The main challenge was to create a dense virtual array only using a very small number of transmitters. The developed design combines an array created from two 4-channels receiver arrays. Both subarrays can be realized using a single 4 channel MMIC. They are showing a square shape while being turned to each-other by 45 degrees. The transmitters are placed below the receiver subarrays, being aligned with their center points. The virtual array is formed by the convolution of transmitter and receiver elements. Due to the alignment of receiver subarrays and transmitters the combination of both receiver squares forms a circular topology on the center of the virtual array with a diameter of 1 cm. This circular array represents the measurement of the signal of the left transmitter measured by the receivers on the right and vice-versa. It is dense enough to provide sufficient side-lobe suppression. Simulations have clearly shown that the outer subarrays formed in the virtual array raise the sidelobe level due to their large separation from the central array. For imaging only the central circular array is used.

Figure 11 shows the compact MIMO camera module with integrated backend and FPGA. The analogue to digital converted data is sended to the processing computer using Gigabit Ethernet. The Ethernet connector is an X-coded female connector and capable of 1000 Mbit/s. The dimension of this MIMO camera are  $5\text{ cm} \times 5\text{ cm}$ .

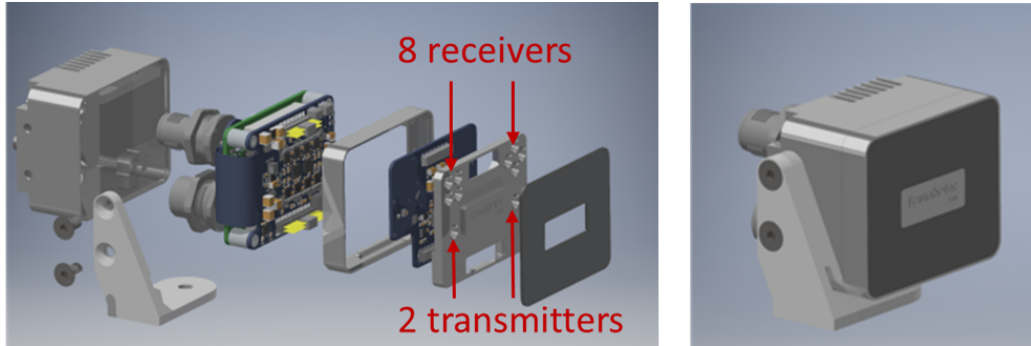


Figure 11: MIMO-Camera: exploded-drawing (left), compact Module (right)

### 3.4. Simulation

The far field point spread function presented in Figure 12 shows a clear central peak in the center of the image. Due to the circular shape of the array the far field can be approximated by a zeroth order Bessel function. Therefore, a ring shaped sidelobe occurs around the center. This sidelobe is only suppressed by 7 dB. However, the field of view restriction to 30 degrees in elevation and azimuth promises to significantly increase sidelobe suppression. For higher look angles sidelobes caused by higher order Bessel functions occur. The directivity of the radiating elevation elements are expected to provide sufficient suppression of these higher order peaks. Of course the resolution is restricted due to the small size of the virtual array. For cause imaging, or better to say, direction estimation this radiation pattern should still be highly suitable. Taking the compact footprint of the array and the small number of channels into account, this design is already highly interesting for a high number of applications in robotics.

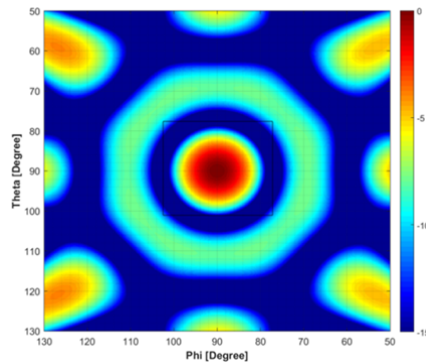


Figure 12: MIMO-Camera: Far field point spread function of radar camera

## 4. Conclusion

This paper presented different kind of radar systems for robotic mapping and localization as well as for security scan applications. The functionality of the 2D mechanically pivoting radar was presented. In the measurement setup the MPR shows with a range resolution of 3 cm and a angular resolution of 1.8° sufficient results. By comparing the MPR data with a LiDAR data inside artificial smoke, the radar system was able to detect the walls of the measured szenario, where the LiDAR system detects ghost targets due to the present of fog.

For 3D imaging two approaches have been presented, a mechanically driven synthetic aperture scanner and a highly compact MIMO array. The 3D SAR scan module operates with one radar element and delivers high resolution images.

However, the measurement time is within a range of several minutes. Real time measurements can be performed using antenna arrays. A MIMO array with 16 channels completely integrated in a 5 cm small package was presented. Even in that tiny form factor an angular resolution of about 10° was obtained. The topology as well as the simulation of the far field point spread function of the 3D MIMO camera was presented. The point spread function shows sufficient suppression for imaging use of the inner central circular array. Therefore, different technological approaches have been demonstrated for equipping future systems with highly compact radar modules to integrate millimeter wave imaging in various applications ranging from robotic environmental screening to security scans.

## Acknowledgement

This work has partly been supported within H2020-ICT by the European Commission under grant agreement number 645101 (SmokeBot).

## References

- [1] Adams, M.; Mullane, J.; Jose, E.:Robotics Navigation and Mapping with Radar. Artech House, 2012
- [2] Herschel, R.; Lang, S. A.; Pohl, N., “Sensor Fusion Supporting High Resolution Radar for Security Applications”, *Proceedings of the 11th Security Research Conference Future Security, 2016*
- [3] Haegelen, M.; Stanko, S.; Essen, H.; Briese, G.; Schlechtweg, M.; Tessmann, A., “A 3-D millimeterwave luggage scanner”, *Infrared, Millimeter and Terahertz Waves, 2008. IRMMW-THz 2008. 33rd International Conference on*, 15-19 Sept. 2008
- [4] Pohl, N.; Jaeschke, T.; Aufinger, K., “An Ultra-Wideband 80 GHz FMCW Radar System Using a SiGe Bipolar Transceiver Chip Stabilized by a Fractional-N PLL Synthesizer”, *Microwave Theory and Techniques, IEEE Transactions on*, March 2012, vol. 60, no. 3, pp. 757-765
- [5] Fritzsche, P.; Kueppers, S.; Briese, G.; Wagner, B., “Radar and LiDAR Sensorfusion in Low Visibility Environments”, *Proceedings of the 13th International Conference on Informatics in Control, Automation and Robotics,(ICINCO) 2016*, vol. 2, pp. 30-36